



RESEARCH ARTICLE

Engineering a monobody specific to monomeric Cu/Zn-superoxide dismutase associated with amyotrophic lateral sclerosis

Hiroshi Amesaka¹ | Mizuho Hara¹ | Yuki Sakai¹ | Atsuko Shintani² |
Kaori Sue² | Tomoyuki Yamanaka³ | Shun-ichi Tanaka¹  |
Yoshiaki Furukawa² 

¹Department of Biomolecular Chemistry,
Kyoto Prefectural University, Kyoto,
Japan

²Department of Chemistry, Keio
University, Yokohama, Japan

³Department of Neuroscience of Disease,
Brain Research Institute, Niigata
University, Niigata, Japan

Correspondence

Shun-ichi Tanaka, Department of
Biomolecular Chemistry, Kyoto
Prefectural University, 1-5
Shimogamohangi-cho, Sakyo, Kyoto
606-8522, Japan.
Email: stanaka1@kpu.ac.jp

Yoshiaki Furukawa, Department of
Chemistry, Keio University, 3-14-1
Hiyoshi, Kohoku, Yokohama, Kanagawa
223-8522, Japan.
Email: furukawa@chem.keio.ac.jp

Funding information

Grants-in-Aid for Scientific Research on
Innovative Areas, Grant/Award Numbers:
19H05765, 20H05516; Scientific Research
(B), Grant/Award Number: 22H02768;
Scientific Research (C), Grant/Award
Number: 21K05386; Ministry of
Education, Culture, Sports, Science and
Technology of Japan, Grant/Award
Number: 22K19389

Review Editor: Aitziber L. Cortajarena

Abstract

Misfolding of mutant Cu/Zn-superoxide dismutase (SOD1) has been implicated in familial form of amyotrophic lateral sclerosis (ALS). A natively folded SOD1 forms a tight homodimer, and the dimer dissociation has been proposed to trigger the oligomerization/aggregation of SOD1. Besides increasing demand for probes allowing the detection of monomerized forms of SOD1 in various applications, the development of probes has been limited to conventional antibodies. Here, we have developed Mb(S4) monobody, a small synthetic binding protein based on the fibronectin type III scaffold, that recognizes a monomeric but not dimeric form of SOD1 by performing combinatorial library selections using phage and yeast-surface display methods. Although Mb(S4) was characterized by its excellent selectivity to the monomeric conformation of SOD1, the monomeric SOD1/Mb(S4) complex was not so stable (apparent $K_d \sim \mu\text{M}$) as to be detected in conventional pull-down experiments. Instead, the complex of Mb(S4) with monomeric but not dimeric SOD1 was successfully trapped by proximity-enabled chemical crosslinking even when reacted in the cell lysates. We thus anticipate that Mb(S4) binding followed by chemical crosslinking would be a useful strategy for in vitro and also ex vivo detection of the monomeric SOD1 proteins.

KEYWORDS

amyotrophic lateral sclerosis, biolayer interferometry, chemical crosslinking, Cu/Zn-superoxide dismutase, monobody, phage display

This is an open access article under the terms of the [Creative Commons Attribution-NonCommercial-NoDerivs](https://creativecommons.org/licenses/by-nc-nd/4.0/) License, which permits use and distribution in any medium, provided the original work is properly cited, the use is non-commercial and no modifications or adaptations are made.

© 2024 The Authors. *Protein Science* published by Wiley Periodicals LLC on behalf of The Protein Society.

1 | INTRODUCTION

Mutations in the gene coding Cu/Zn-superoxide dismutase (SOD1) link to a familial form of amyotrophic lateral sclerosis (ALS) (Rosen et al., 1993), and abnormal accumulation of misfolded SOD1 proteins in the affected sites such as spinal motor neurons is a pathological hallmark (Bruijn et al., 1998). It remains controversial whether misfolded SOD1 *in vivo* as well as *in vitro* is toxic to cells (Hayashi et al., 2016). For the understanding of a pathomechanism of ALS, therefore, it is important to investigate how SOD1 becomes misfolded in the affected tissues.

Notably, SOD1 is an extremely stable metalloprotein characterized by the melting temperature (T_m) of about 90°C and thus appears to be resistant to the misfolding under physiological conditions (Forman & Fridovich, 1973). Such high stability of SOD1 is known to be realized largely by binding metal ions (Furukawa & O'Halloran, 2005); as shown in Figure 1, SOD1 is a homodimer, and each of the subunits binds a copper and zinc ion. Upon losing the bound metal ions, indeed, SOD1 decreases its high thermostability, which could thus increase the chance of SOD1 to misfold into abnormal oligomers/aggregates at the physiological temperature (Furukawa, 2021). Furthermore, the increasing fraction of SOD1 is considered to become monomerized *in vitro* upon denaturational stresses including pathogenic mutations (Khare et al., 2004; Lindberg et al., 2005;

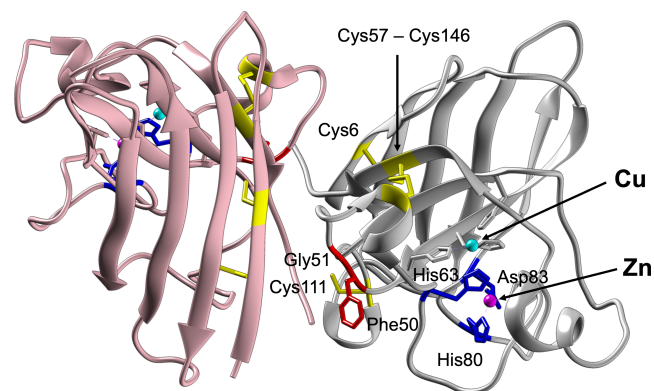


FIGURE 1 A structure of human SOD1 (PDB ID: 1HL5) The subunits of the SOD1 homodimer are colored pink and gray. The bound copper and zinc ion in each subunit are shown as a cyan and magenta sphere, respectively. Also, the conserved intramolecular disulfide bond between Cys57 and Cys146 is shown. In SOD1(MM), all four Cys residues (Cys6, 57, 111, 146) colored yellow and three residues ligating the zinc ion (His63, 80, Asp83) colored blue are replaced with Ser and Ala, respectively (i.e., C6S/C57S/C111S/C146S/H63A/H80A/D83A). In SOD1(FG), Glu is substituted for Phe50 and Gly51, shown in red (i.e., F50E/G51E).

Mulligan et al., 2008), implying that the monomerization precedes the misfolding of SOD1. In other words, monomeric SOD1 would serve as an important precursor in the misfolding into oligomers/aggregates.

In spite of such potential relevance of SOD1 monomer in the pathomechanism of ALS, a small population of the monomer ($K_d \sim 0.1$ nM) (Khare et al., 2004) makes it difficult to detect the monomer by conventional methods such as the size-exclusion chromatography; in the chromatogram, an apparently increased fraction of the monomer could be misrepresented by the tailing of the elution peak. For the detection of monomeric SOD1 *in vivo*, the SOD1 exposed dimer interface (SEDI) antibody could be useful, which was raised to a linear epitope constituting of the SOD1 homodimer interface (Rakhit et al., 2007). The epitope is inaccessible in the native, homodimeric conformation of SOD1 but becomes available upon its monomerization and/or denaturation. The SEDI antibody was shown to detect SOD1 denatured *in vitro* by urea and also successfully probe pathological mutant SOD1 in the ALS model mice. While not examined in detail, the ability of the SEDI antibody to detect monomerized SOD1 *in vivo* as well as *in vitro* is expected; however, the SEDI antibody is polyclonal and could hence be difficult to obtain reproducible results.

Conventional antibodies produced via a natural infection system are often the primary choice for applications in the fields of biology and medicine, but an alternative class of affinity reagents has also emerged in the form of recombinant antibodies and synthetic binding proteins built with non-antibody scaffolds (Helma et al., 2015). These binders can be prepared as completely recombinant proteins with their gene sequences known and cloned, making them inapprehensive of the reproducibility problem of polyclonal antibodies. Through *in vitro* screening of combinatorial libraries using phage and yeast-surface display technologies, it is possible to generate desired binders with high specificity for diverse targets (Sha et al., 2017). In contrast to traditional antibodies, recombinant binders generated *in vitro* offer control over the conformational state of the target protein. This is of particular advantage when seeking an affinity reagent that selectively recognizes a specific conformation of the target protein versus alternative one(s). One of the well-established platforms for generating synthetic binding proteins is the monobody technology based on the scaffold of the tenth human fibronectin type III domain (hFN3) (Koide et al., 1998). As described in a recent review and the references therein, a large number of conformation-specific monobodies targeting different states within the conformational ensemble of the target protein have been developed (Hantschel et al., 2020). In addition to these precedents, we recently demonstrated the development of monobodies highly

specific to the respective conformation states using the example of *Escherichia coli* adenylate kinase with a large conformational change between OPEN and CLOSED forms (Nakamura et al., 2023).

In this study, we succeeded in the generation of a monobody (Mb(S4)) exclusively recognizing monomeric but not dimeric SOD1. While the complexation of monomeric SOD1 with recombinant Mb(S4) was characterized by the moderate affinity ($K_d \sim 10^{-6}$), the specific complex of monomeric SOD1 with Mb(S4) was able to be trapped through the proximity-enabled chemical cross-linking with bis(sulfosuccinimidyl)suberate. Moreover, we found that Mb(S4) was successfully applied to the detection of monomeric SOD1 in the lysates of cells expressing ALS-causing mutant human SOD1. A structural rationale for the discrimination of SOD1 monomer by Mb(S4) is also discussed. The crosslinking with Mb(S4) is hence considered to be a novel and convenient method to evaluate the monomerization of SOD1 in the samples *ex vivo* as well as *in vitro*.

2 | MATERIALS AND METHODS

Preparation of recombinant SOD1 proteins, Preparation of recombinant monobody proteins, Competition binding assay, Analysis of the SOD1 quaternary structure with multiangle light scattering (MALS), Budding yeast cells expressing human SOD1 proteins, and Preparation of lysates from cultured cells expressing human SOD1 proteins are described in the Supplemental Experimental Procedures S1.

2.1 | Monobody generation

The monobody side library used and general selection methods have been described previously (Koide et al., 2012; Tanaka et al., 2015, 2018), except that the CD- and FG-loops were diversified by NNC (where N is A, T, G, or C) randomization instead of a biased amino-acid composition design. The buffers used for binding reaction and washing were TBSB (20 mM Tris-HCl pH 7.4, containing 150 mM NaCl and 1 mg/mL bovine serum albumin [BSA]) and TBSBT (TBSB and 0.1% (v/v) Tween 20), respectively, for phage display selection experiments. Four rounds of phage display selection against the biotinylated His₁₀-Avi-SOD1 (MM) were performed. The target concentrations used for rounds 1–2 and 3–4 were 100 and 50 nM, respectively. Monobody-displayed phages were captured onto the biotinylated target immobilized to streptavidin-coated magnetic beads (Z5481/2, Promega) and then eluted in 0.1 M

Gly-HCl, pH 2.1. After gene shuffling among phage clones within each enriched population and transfer of the resulting gene pool to a yeast surface display vector, we performed two rounds of library sorting by yeast-surface display using the target concentrations of 500 nM. These sorting experiments were performed as described previously (Tanaka et al., 2015, 2018), except that DyLight 650-conjugated streptavidin (Abcam) (or NeutrAvidin [Invitrogen]) and FITC-conjugated goat anti-mouse IgG (BioLegend) were used as the secondary detection reagents for the biotinylated His₁₀-Avi-SOD1 (MM) and the surface-displayed monobodies, respectively.

2.2 | Binding analysis for monobodies using yeast-surface display

Affinity and specificity of the generated monobodies against on-target (biotinylated His₁₀-Avi-SOD1(MM) or biotinylated His₆-SOD1(MM)-Avi) and off-target (biotinylated SOD1(WT)-His₆-Avi) proteins were assessed using yeast-surface display as described previously (Fujita et al., 2023). In brief, yeast cells displaying a monobody were incubated with varying concentrations of the biotinylated SOD1, washed with the buffer and stained with fluorescently labeled secondary detection reagents, prior to analysis on a Muse flow cytometer (Millipore). The secondary detection reagents used were DyLight 550-conjugated streptavidin (abcam) and PerCP-conjugated goat anti-mouse IgG (BioLegend) for the biotinylated SOD1 and the surface-displayed monobodies, respectively. K_d values were determined from plots of the median fluorescent intensity against SOD1 concentration by fitting the 1:1 binding model using SigmaPlot software ver. 15.0 (Systat Software). For the epitope mapping of monobodies, four variants of His₆-SOD1(MM)-Avi, namely I17R, D96R, E133A and R143A, were used as target proteins at a concentration of 2 μ M. For analyzing the paratope on the monobodies, a point mutation was introduced into the monobody gene in the yeast surface display vector, and the resultant plasmid was then used to transform *S. cerevisiae* EBY100 Strain. The His₆-SOD1 (MM)-Avi concentration used for this analysis was 2 μ M.

2.3 | Analysis of the SOD1–monobody interaction with BLI

The kinetics of the binding of SOD1 proteins with monobodies were measured with a BLItz™ instrument (Sartorius). Biosensors coated with streptavidin were soaked for at least 10 min in a BLI assay buffer (pH 7.0)

containing 50 mM MOPS, 100 mM NaCl, 1 mM EDTA, 1% BSA, and 0.02% Tween 20. The biosensors were set to the instrument, soaked in the BLI assay buffer containing monobody for 120 s, and washed with the BLI assay buffer for 60 s. Those monobody-loaded biosensors were then used for the binding assay, which consisted of the following three steps: the initial baseline step using the BLI assay buffer (60 s), the association step using 1, 5, 10, 50 μ M SOD1 in the BLI assay buffer (120 s), and the dissociation step using the BLI assay buffer (120 s). The observed sensorgrams were attempted to be fit to a 1:1 binding model using a BLItz Pro software version 1.2 (Sartorius).

2.4 | Analysis of the SOD1-Mb(S4) interaction with chemical crosslinkers

Recombinant SOD1 proteins (15 μ M) and the *S. cerevisiae*/*E. coli*/Neuro2a cell lysates (also see the legend of Figure 6) were mixed with 15 μ M biotinylated Mb(S4) with a C-terminal Avi-tag in the MN buffer, to which a crosslinker BS3 (Bis(sulfosuccinimidyl)suberate disodium salt, DOJINDO) dissolved in water was added (final concentration, 1 mM). After incubation at room temperature for 30 min, 1 M Tris at pH 8 was added to the samples (final concentration of Tris, 50 mM) to stop

the crosslinking reactions. The samples were further mixed with the Laemmli sample buffer containing β -mercaptoethanol and analyzed with SDS-PAGE using 12.5% polyacrylamide gels. For the analysis using recombinant SOD1 proteins, the gels were stained with Coomassie Brilliant Blue R-250; for the analysis using the *S. cerevisiae*/*E. coli*/Neuro2a cell lysate samples, the proteins separated on the gel by SDS-PAGE were electroblotted on a PVDF membrane, and examined by Western blotting using the polyclonal antibody against SOD1 (GeneTex, No. GTX100554).

3 | RESULTS AND DISCUSSION

3.1 | Models of monomeric SOD1 by amino acid substitutions

As mentioned in Introduction, SOD1 is known to exist as a tight homodimer (also see Figure 1). Indeed, irrespective of the presence or absence of copper and zinc ions, wild-type (WT) SOD1 was eluted from a gel-filtration column as a single peak and estimated to have \sim 27 kDa of the molar mass by multi-angle light scattering coupled with size exclusion chromatography (SEC-MALS), which was close to the calculated mass of the dimer (31,872) (Figure 2a–c). A slightly smaller mass (21,300) of SOD1

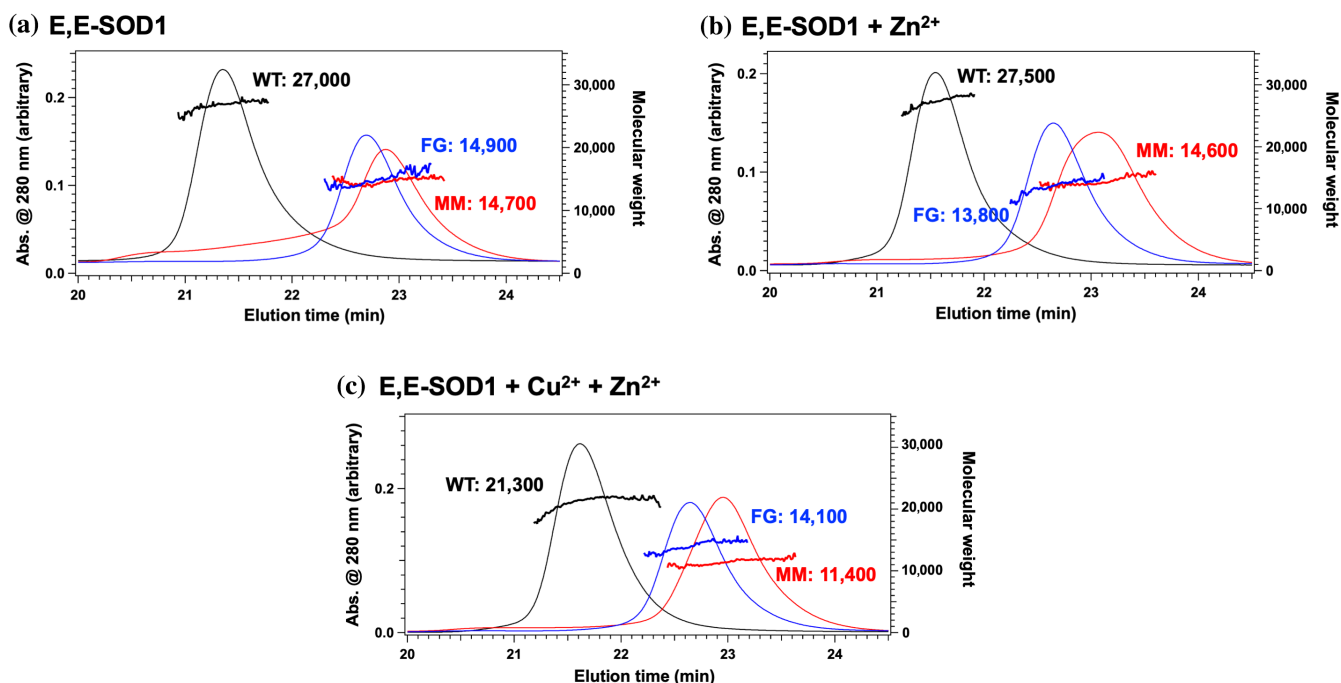


FIGURE 2 Experimental models of monomeric SOD1 with the amino acid substitutions The monomer/dimer state of SOD1 was examined by SEC-MALS: black, SOD1(WT); red, SOD1(MM); blue, SOD1(FG). The chromatograms monitored at 280 nm (left axis) were shown together with the plots of the molecular weight calculated from the MALS analysis (right axis). Samples contained 50 μ M SOD1 proteins in the MN buffer, where 5 mM EDTA was further included for the analysis of E,E-SOD1. (a) E,E-SOD1, (b) E,E-SOD1 with equimolar Zn²⁺, (c) E,E-SOD1 with equimolar Cu²⁺ and Zn²⁺.

(WT) was estimated in the presence of Cu^{2+} (Figure 2c); this was considered to be underestimated due to the absorption of the protein-bound Cu^{2+} at 280 nm. The elution time of SOD1(WT) with Cu^{2+} and Zn^{2+} was not significantly different from those of SOD1 lacking both of the metal ions (designated as E,E-SOD1) and also of SOD1(WT) with Zn^{2+} . We thus confirmed that SOD1 (WT) existed dominantly in the homodimeric state.

It has been shown that E,E-SOD1 is monomerized upon further reduction of the conserved intramolecular disulfide bond between Cys57 and Cys146 (Arnesano et al., 2004; Furukawa et al., 2004). As a model of monomeric SOD1, we thus prepared mutant SOD1 (SOD1 (MM)) in which all four Cys residues (Cys6, 57, 111, 146) were replaced with Ser, and alanine was further substituted for two of the four Zn^{2+} ligands (His80 and Asp83) and the bridging ligand binding both Cu^{2+} and Zn^{2+} (His63). Another model of monomeric SOD1 in this study was the SOD1 variant (SOD1(FG)) by substituting Glu for Phe50 and Gly51, which locate at the dimer interface (Bertini et al., 1994). To test if those two monomeric SOD1 variants were indeed monomeric, the analysis with SEC-MALS was performed. Both SOD1(MM) and SOD1 (FG) were found to be eluted later compared with SOD1 (WT) and estimated to have ~15 kDa of the molar mass, which corresponds to the calculated mass of the monomer (Figure 2a–c). While E,E-SOD1(MM) would distribute to dimeric species albeit not a distinct elution peak (Figure 2a), our two monomeric SOD1 variants were confirmed to remain dominantly monomeric both in the presence and absence of copper/zinc ions.

3.2 | Generation of monobodies recognizing monomeric but not dimeric SOD1

To generate monobodies that recognize monomeric SOD1, we performed selections against the biotinylated His₁₀-Avi-SOD1(MM) (see Section 4) using the monobody side library (Figure 3a). After four rounds of library selection by phage display, the enriched clones were subjected to gene shuffling, and the resulting gene pool was transferred into a yeast-surface display format for further selection. Three out of eight isolates exhibiting strong binding to the biotinylated SOD1(MM) at the target concentration of 1.0 μM were selected for sequencing. From these sequencing reads, we identified two unique clones (Mb(S1) and Mb(S2) in Figure 3b). It is noted that the DE-loop of Mb(S1) had unexpected mutations (GSKS to GYYS), which probably occurred during PCR-amplification of the enriched clones' genes for gene shuffling. Measurements of the apparent equilibrium

dissociation constant (K_d) using the yeast-surface display format revealed that both clones had K_d values in the hundreds nanomolar range to the biotinylated SOD1 (MM) (Figure 3c). Of the two, Mb(S1), but not Mb(S2), showed undetectable binding to the biotinylated SOD1 (WT). Consistent results were obtained by competition binding assay, where the effects of non-tagged SOD1 (WT) or SOD1(MM) on the interaction between biotinylated SOD1(MM) and Mb were tested (Figure 3d), indicating that Mb(S1) is highly specific to the monomeric SOD1. Despite the high specificity, Mb(S1) bound weakly to the monomeric SOD1. Therefore, we attempted to improve the affinity of Mb(S1) by error-prone PCR and directed evolution techniques, yielding two new monobodies, Mb(S3) and Mb(S4), showing higher affinity with preserving the desired specificity profile of Mb(S1) (Figure 3b–d). Notably, only one amino acid (the residue at position 78) was found to be different between Mb(S1) and Mb(S4), which was Phe and Tyr, respectively (Figure 3b). Given the higher affinity of Mb(S4) to SOD1 (MM) than that of Mb(S1), Y78 in Mb(S4) would be involved in the interaction with SOD1(MM), which will be discussed later. Because Mb(S4) showed higher expression yield as a soluble protein than Mb(S3) (~10 and 3 mg from 1L culture for Mb(S4) and Mb(S3), respectively: see Figure S1), we selected Mb(S4) for further characterization.

3.3 | Characterization of the specific interaction of Mb(S4) with monomeric SOD1

We analyzed the interaction between Mb(S4) and SOD1 proteins with biolayer interferometry (BLI). For this purpose, Mb(S4) with the N-terminal His₆ tag was biotinylated through the Avi-tag at the C-terminus (His₆-Mb (S4)-Avi) and fixed at the tip of a biosensor coated with streptavidin. The biosensor was first immersed in an analyte solution (i.e., SOD1 samples), and the association kinetics between Mb(S4) and SOD1 were monitored. The biosensor was then immersed in the buffer, allowing us to monitor the dissociation kinetics. Figure 4a shows the sensorgrams of the interaction between Mb(S4) and E,E-SOD1(MM), and the concentration-dependent increase of the binding in the association step was observed. As a negative control, sh-hFN3, the shaved hFN3 scaffold where the amino acids in the FG-loop have been mutated to serines (Figure 3b), was also evaluated. We then confirmed that biosensors loaded with sh-hFN3 or left unloaded exhibited negligible binding with E,E-SOD1 (MM) (Figure 4c,d). These results supported the formation of the Mb(S4)/E,E-SOD1(MM) complex; nonetheless,

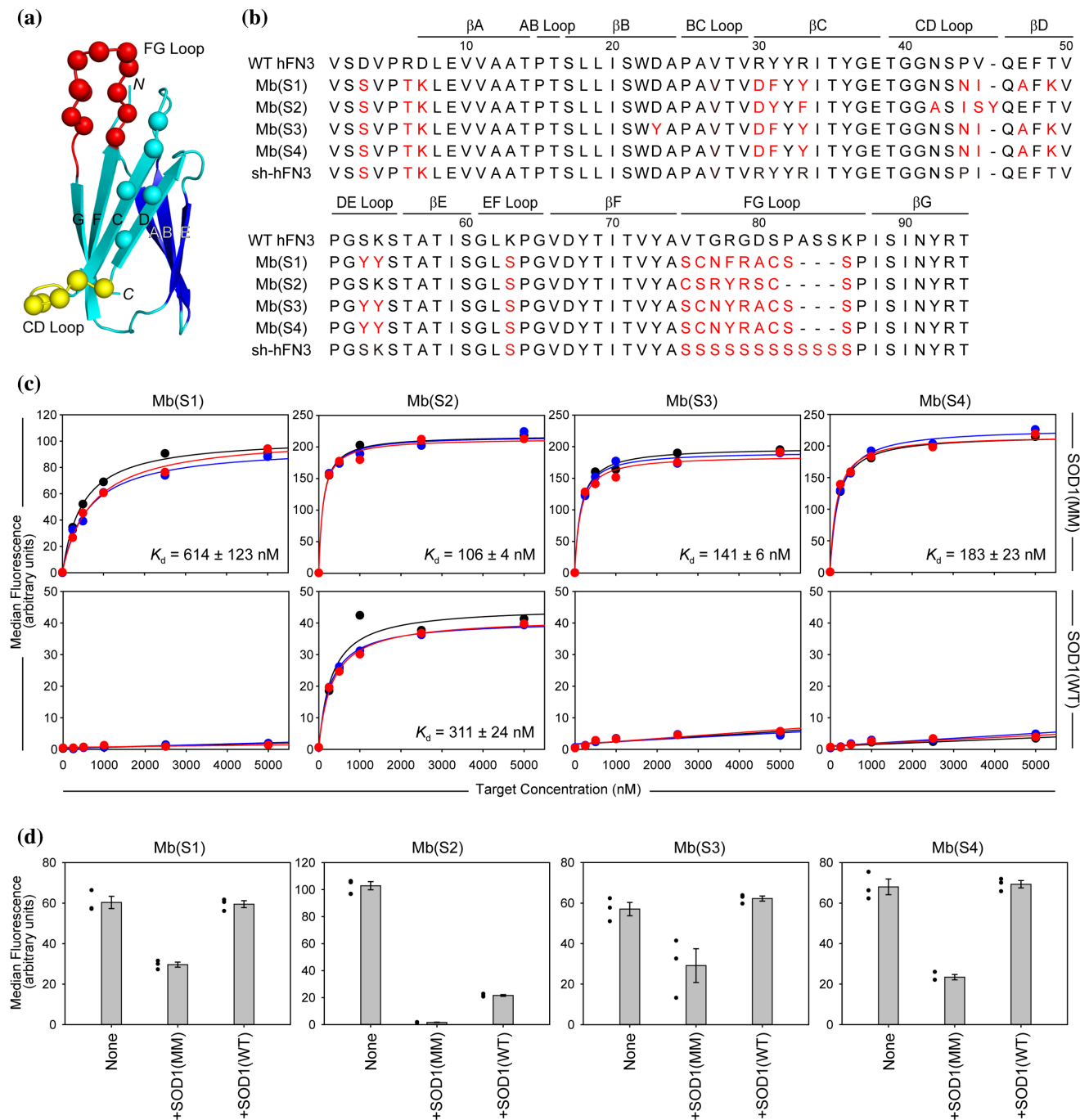


FIGURE 3 Generation of monobodies binding to SOD1. (a) Schematic of the hFN3 scaffold with the locations of diversified residues in the side library shown as spheres. The strands, loops, and termini are labeled. (b) Amino acid sequences of the wild-type hFN3, sh-hFN3, and generated monobodies (Mb(S1)–Mb(S4)). Mutated residues are colored in red. (c) Binding titration curves and the dissociation constants (K_d) of the monobodies toward biotinylated His₁₀-Avi-SOD1(MM) (upper panels) and biotinylated SOD1(WT)-His₆-Avi (lower panels) measured using yeast-surface display. The median fluorescence intensities are plotted as a function of SOD1 concentration. The K_d values and errors shown are mean and standard deviations of three independent measurements. (d) Binding of monobodies indicated above each panel to biotinylated His₁₀-Avi-SOD1(MM) in the absence and presence of competitor non-tagged SOD1 proteins is shown. Biotinylated His₁₀-Avi-SOD1(MM) concentrations used were 500 nM for Mb(S1) and 150 nM for other monobodies, respectively. The concentrations of competitor non-tagged SOD1 proteins used were 10 μ M for Mb(S1) and 5 μ M for other monobodies, respectively. Values are shown as the mean of three independent experiments with standard deviation.

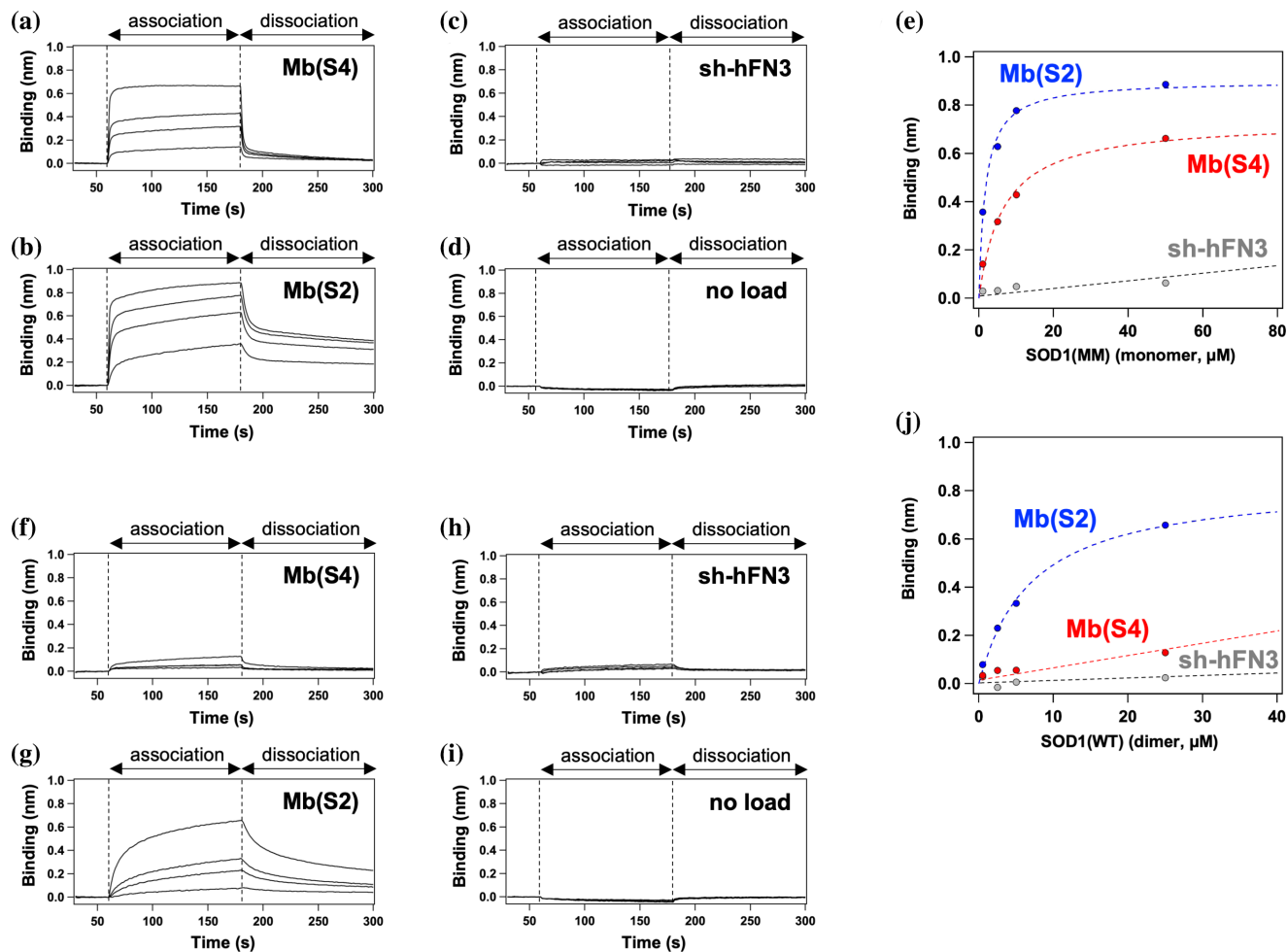


FIGURE 4 BLI analysis on interaction of monobodies with monomeric and dimeric SOD1 (a–d, f–i) BLI sensorgrams obtained using (a,f) His₆-Mb(S4)-Avi-loaded, (b,g) His₆-Mb(S2)-Avi-loaded, (c,h) His₆-sh-hFN3-Avi-loaded, and (d,i) unloaded biosensors with the solutions of 1, 5, 10, and 50 μM SOD1 proteins (a–d, E,E-SOD1(MM); f–i, E,E-SOD1(WT)) were shown. The dotted lines indicate the start of the association and dissociation phases. The observed binding signals in the association step became higher as the concentration of SOD1 increased. (e,j) The binding signals at the end of the association phase were plotted against the concentration of (e) SOD1(MM) and (j) SOD1 (WT): red, Mb(S4); blue, Mb(S2); gray, sh-hFN3. The fit of the plots to a 1:1 binding model was also shown as broken curves.

both association and dissociation occurred too rapidly to estimate the rate constants and the dissociation constant (K_d) by the global fitting of the sensorgrams to a 1:1 binding model. Instead, K_d was estimated to be $\sim 5 \times 10^{-6}$ M, as derived from the dependence of the binding signal in the association step on the concentration of E,E-SOD1 (MM) (Figure 4e).

To elucidate the specificity of Mb(S4) for monomeric SOD1, the binding of Mb(S4) toward E,E-SOD1(WT), which predominantly exists as the homodimeric state (Figure 2a), was examined with BLI. As shown in Figure 4f, the binding signals were significantly smaller than those observed between Mb(S4) and E,E-SOD1 (MM) (Figure 4a). Again, we confirmed no binding signals of E,E-SOD1(WT) with the biosensors loaded with sh-hFN3 or left unloaded (Figure 4h,i). These findings

support the preference of Mb(S4) for binding to the monomeric state of SOD1 rather than its dimeric counterpart.

We also analyzed the interaction of Mb(S4) with another model of monomeric SOD1, SOD1 (FG) (Figure 2c). Rapid increase and decrease of the binding signals were observed in the association and dissociation step, respectively (Figure S2A); however, the signal of SOD1(FG) gradually increased during the association step and did not return to the baseline in the dissociation step. Those changes in the binding signals were also observed in the analysis of SOD1(FG) using the biosensors loaded with sh-hFN3 or left unloaded (Figure S2C,D), indicating the non-specific adsorption of SOD1(FG) to the biosensors. Although the binding parameters were difficult to be estimated, the rapid

increase and decrease of the binding signals in the association and dissociation step were considered to represent the interaction of Mb(S4) with SOD1(FG).

To further highlight the specificity of Mb(S4) for monomeric SOD1, we compared its binding behavior with that of Mb(S2) using BLI. Our yeast-surface display analysis has suggested that, unlike Mb(S4), Mb(S2) is capable of binding to both monomeric and dimeric SOD1 proteins (Figure 3c). The sensorgrams in Figure 4b demonstrate that Mb(S2) increased the binding signal with E,E-SOD1(MM) in its concentration-dependent manner, confirming its ability to bind to the monomeric state of SOD1. Nonetheless, the association phase was characterized by a rapid initial increase in signal intensity, followed by a more gradual rise; in the dissociation phase, there was a decrease in the signal, which did not revert to baseline levels (Figure 4b). These sensorgram patterns may thus reflect complex binding kinetics between Mb(S2) and E,E-SOD1(MM) or potential non-specific interactions. While the sensorgrams were not described simply by the 1:1 binding model, we obtained an apparent K_d of $\sim 2 \times 10^{-6}$ M by the plot of the binding signals against the concentration of E,E-SOD1(WT) (Figure 4e). Mb(S2) was also considered to bind monomeric SOD1 (FG), but the interaction was again difficult to be quantitatively analyzed due to the non-specific adsorption of SOD1(FG) on the biosensor (Figure S2B).

Unlike Mb(S4), Mb(S2) produced binding signals with E,E-SOD1(WT). Compared with the interaction

with monomeric SOD1, Mb(S2) was found to bind E,E-SOD1(WT) with slower association and dissociation kinetics (Figure 4g). While the sensorgrams did not conform well to a simple 1:1 binding model, an apparent K_d of 7×10^{-6} M was deduced from the dependence of the signals on the E,E-SOD1(WT) concentration (Figure 4j).

Taken together, Mb(S4) interacted specifically with the monomeric but not dimeric state of SOD1, but the complex between Mb(S4) and monomeric SOD1 was found not to be so stable ($\sim 10^{-6}$ M of apparent K_d) for the detection of monomeric SOD1 in conventional methods such as a pull-down assay.

3.4 | Detection of monomeric SOD1 by chemical crosslinking with Mb(S4)

In seeking to develop a viable method for the detection of monomeric SOD1 with Mb(S4), we attempted to stabilize or trap the complex of Mb(S4) with monomeric SOD1 by chemical crosslinking. Disuccinimidyl glutarate (DSG) and bis(sulfosuccinimidyl)suberate (BS3) are homobifunctional crosslinking agents that contain amine-reactive ester groups at each end. With these agents, crosslinking reaction occurs only when the two molecules are in close proximity to each other. As shown in Figure 5a (lanes 5 and 8), the mixtures of E,E-SOD1(MM, FG) and Mb(S4) produced a new band at ~ 30 kDa upon treatment with BS3. The treatment with DSG also led to

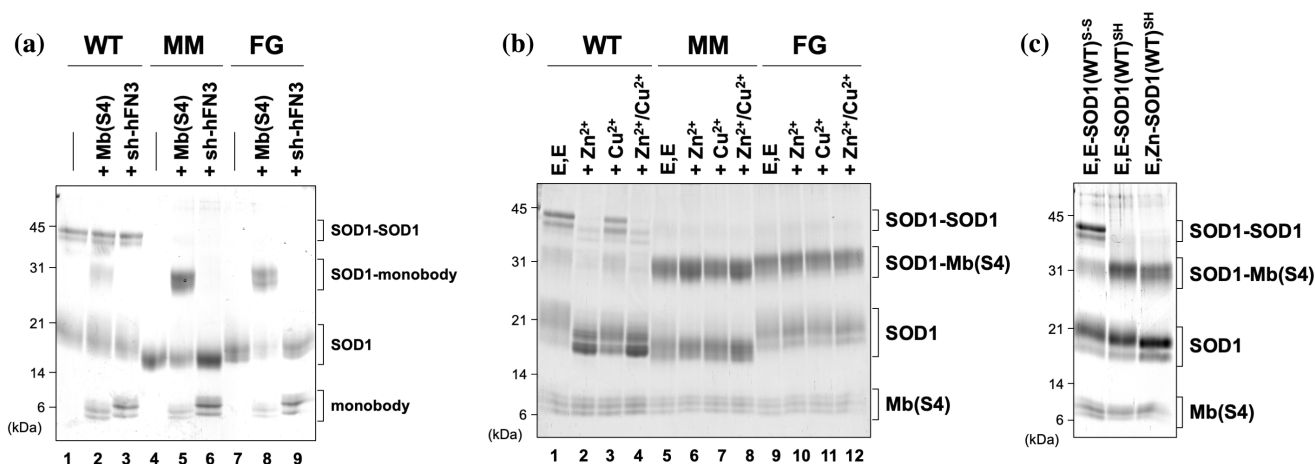


FIGURE 5 SDS-PAGE analysis on the specificity of chemical crosslinking of monomeric SOD1 with Mb(S4) (a) Cross-linking reactions were examined with 15 μM E,E-SOD1(WT, MM, FG) with 1 mM crosslinker (BS3) in the presence or absence of either 15 μM biotinylated Mb(S4) or sh-hFN3 with a C-terminal Avi-tag. (b) Effects of a copper and zinc ion on the crosslinking reactions of SOD1 with Mb(S4) were examined. In addition to the apo state (indicated as E,E), SOD1(WT, MM, FG) proteins with an equimolar amount of either Zn²⁺, Cu²⁺, or both were mixed with biotinylated Mb(S4) with a C-terminal Avi-tag, and the mixtures were reacted with the crosslinker, BS3. The reaction conditions were essentially the same with those in (a). (c) Effects of the disulfide reduction in SOD1 on the crosslinking between SOD1 and Mb(S4) were examined. The apo-form of SOD1(WT) with the disulfide bond is designated as E,E-SOD1(WT)^{S-S}, while the disulfide-reduced form is E,E-SOD1(WT)^{SH}. Also, E,E-SOD1(WT)^{SH} with equimolar Zn²⁺ is indicated as E,Zn-SOD1(WT)^{SH}. The reaction conditions were again essentially the same with those in (a).

the formation of the band at ~ 30 kDa (lanes 6 and 9 in Figure S3). This band was not observed when E,E-SOD1 (MM and FG) or Mb(S4) was reacted individually with the crosslinking agents (lanes 4 and 7 in Figure 5a; lanes 1 and 2 in Figure S3). Furthermore, the cross-linking reaction of sh-hFN3, a monobody as a negative control, with E,E-SOD1(WT, MM, FG) using BS3 did not form the 30 kDa band (lanes 3, 6, and 9 in Figure 5a). Mb(S4) used for the cross-linking reactions was biotinylated, and the 30 kDa band was detected by both anti-SOD1 and anti-biotin antibody (Figure S4); therefore, the band at ~ 30 kDa was considered to represent the crosslinked complex between Mb(S4) and monomeric SOD1. The cross-linking of E,E-SOD1(WT) with Mb(S4) was also examined (lane 2 in Figure 5a; lanes 3 and 4 in Figure S3), but the crosslinked SOD1-Mb(S4) band at ~ 30 kDa was less significant compared with those obtained with SOD1(MM, FG). Because of the homodimeric conformation, E,E-SOD1(WT) was favorably crosslinked with itself by the crosslinking agent (lane 1 in Figure 5a).

Given that the monomer-dimer equilibrium of SOD1 is known to be affected by the binding of a copper and zinc ion (Arnesano et al., 2004; Furukawa et al., 2004; Tajiri et al., 2022), effects of the metal ions on the formation of the crosslinked SOD1-Mb(S4) complex were examined. As shown in Figure 5b (lanes 1–4), the cross-linking of SOD1(WT) with Mb(S4) and also with itself appeared to be slightly retarded in the presence of a zinc but not a copper ion. This is consistent with our recent study showing that the monomer-dimer equilibrium of SOD1(WT) further shifts to the dimer upon the binding of a zinc but not a copper ion (Tajiri et al., 2022). SOD1 (MM, FG) remained monomeric even in the presence of the metal ions (Figure 2); as expected, addition of the metal ions did not affect the formation of the crosslinked complex with Mb(S4) in those monomer models of SOD1 (lanes 5–8 and 9–12 in Figure 5b). Furthermore, it is known that SOD1 becomes monomerized upon reduction of the intramolecular disulfide bond between Cys57 and Cys146 (Arnesano et al., 2004; Furukawa et al., 2004) (Figure 1), and indeed, we confirmed that the crosslinked complex of SOD1(WT) with Mb(S4) was significantly increased by the disulfide reduction (Figure 5c). Taken together, we considered that chemical crosslinking would be an effectual strategy which gives Mb(S4) its applicability to the specific detection of monomeric SOD1.

3.5 | Detection of monomeric SOD1 with Mb(S4) in samples ex vivo

To test if Mb(S4) can detect SOD1 variants even in heterogenous protein mixtures ex vivo, human SOD1 proteins

with ALS-causing mutations were transiently overexpressed in Neuro2a mouse neuroblastoma cells, and the cell lysates were examined by the crosslinking reactions with Mb(S4) or the negative control monobody sh-hFN3. As shown in Figure 6a (upper panel), the crosslinked Mb(S4)-human SOD1 was evident as a band at ~ 30 kDa especially in WT and L144F SOD1 with relatively strong intensity. These crosslinked species were not observed when sh-hFN3 was used (Figure 6a, middle panel). Utilizing the distinct electrophoretic mobilities of SOD1 with and without the disulfide bond, we further examined the thiol-disulfide status of human SOD1 proteins overexpressed in Neuro2a and found a slight amount of SOD1 (WT and L144F, in particular) in the disulfide-reduced state (Figure 6a, lower panel). These results thus suggest that our crosslinking assay with Mb(S4) can detect monomerized SOD1 ex vivo partly due to the absence of the conserved disulfide bond (also see Figure 5c).

Given that the disulfide formation in SOD1 would not efficiently proceed under the condition of the overexpression, the cross-linking assay with Mb(S4) was examined in the lysates of *Saccharomyces cerevisiae* in which the endogenous *sod1* gene was replaced with a cDNA coding human SOD1 variant and thus expressed at a physiological level. As shown in Figure 6b, the crosslinked Mb(S4)-SOD1 band was detected in the *S. cerevisiae* lysates expressing SOD1(A4V) and SOD1(I149T) but was not significant in the others (WT, G37R, G85R, and G93A). Again, the negative control monobody sh-hFN3 did not produce the crosslinked species with SOD1. We also confirmed that the disulfide bond was introduced in virtually all of human SOD1 expressed in our *S. cerevisiae* cells (Figure 6c). These results suggest that the A4V and I149T substitution facilitate the monomerization of SOD1 with the disulfide bond. Ala4 and Ile149 are positioned at the dimer interface, but the others (Gly37, Gly85, and Gly93) are distant from the interface. Indeed, SOD1(A4V) dimer has been experimentally shown to have the increased dissociation constant ($K_d \sim 1 \mu\text{M}$) compared with that of SOD1(WT) (Redler et al., 2011). Taken together, our crosslinking assay validated Mb(S4) as a potent probe for the detection of monomeric SOD1 when expressed at a physiological level.

Moreover, the cross-linking assay was examined using human SOD1 variants overexpressed in *E. coli* SHuffle™ with enhanced capacity to introduce disulfide bonds to proteins in the cytoplasm. The disulfide bond was efficiently introduced to human SOD1 variants (Figure 6c), except for SOD1(C⁴S) variant in which all four Cys (Cys6, 57, 111, 146) are replaced with Ser. As shown in Figure 6d, human SOD1 with G37R, G85R, G93R, and C111Y mutation exhibited the crosslinked Mb(S4)-SOD1 bands with almost comparable intensity to that of SOD1

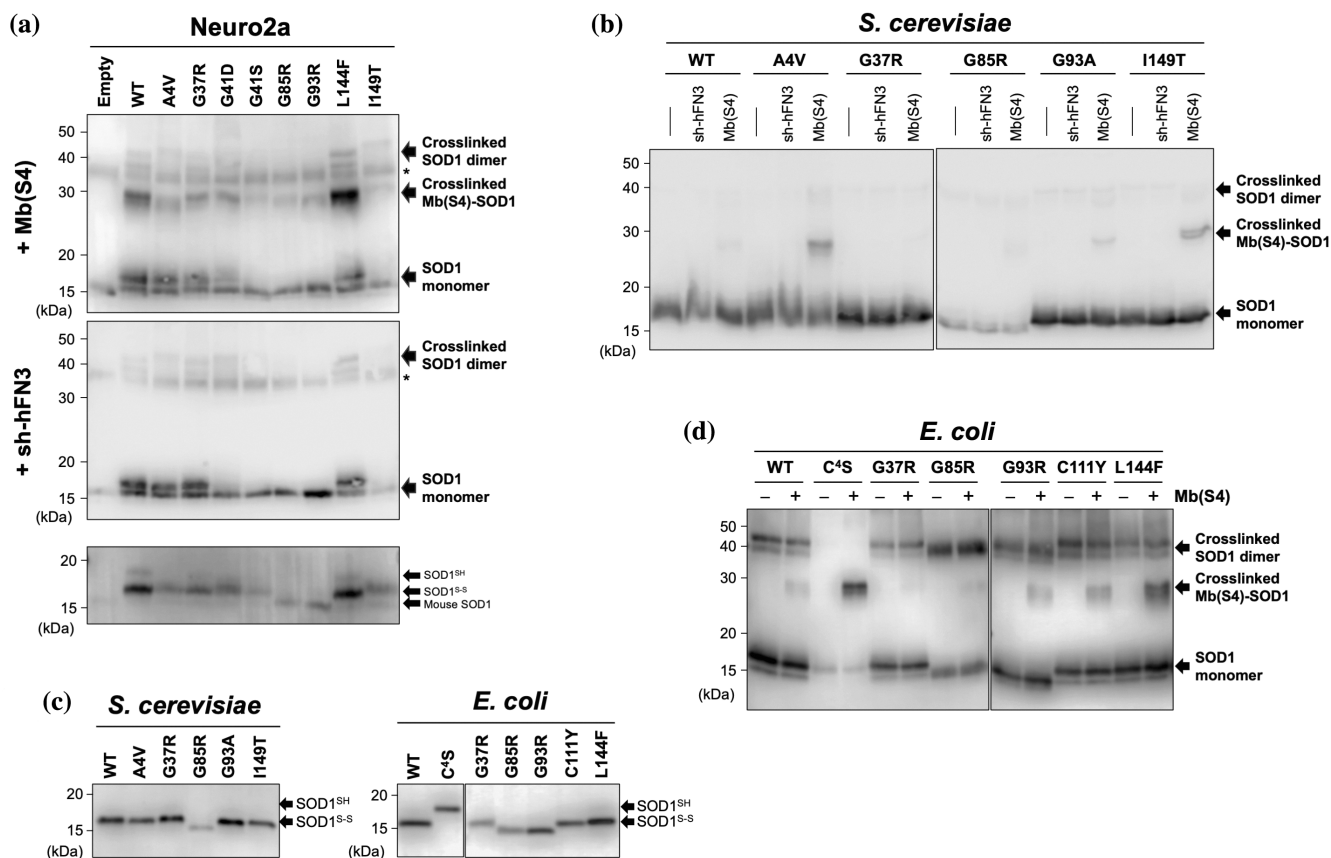


FIGURE 6 Cross-linking detection of monomeric SOD1 with Mb(S4) in samples ex vivo. The lysates of (a) Neuro2a, (b) *S. cerevisiae*, and (d) *E. coli* SHuffle™ expressing human SOD1 proteins (WT and mutants indicated) were treated with 1 mM BS3 in the presence (+) or absence (–) of the indicated monobodies (10 μM). The concentrations of total proteins (excluding monobodies) in the samples from Neuro2a, *S. cerevisiae* and *E. coli* SHuffle™ lysates were 0.80, 0.24, and 0.6 g/L, respectively, and the reaction mixtures containing 10 μg (Neuro2a), 20 μg (*S. cerevisiae*) and 0.04 μg (*E. coli* SHuffle™) of the total proteins (excluding monobodies) were analyzed with Western blotting using anti-SOD1 antibody as a primary antibody. (c) The thiol-disulfide status of SOD1 in cell lysates were also shown. The lysates of (a, lower) Neuro2a, (c, left) *S. cerevisiae*, and (c, right) *E. coli* SHuffle™ were examined by non-reducing SDS-PAGE followed by Western blotting with anti-SOD1 antibody as a primary antibody. The electrophoretic mobility of SOD1 is known to retard upon reduction of the disulfide bond and increase by G85R and G93R mutation. The experiments were repeated at least twice with reproducible results.

(WT), suggesting a limited propensity for these mutant proteins to monomerize. In contrast, the Mb(S4)-SOD1 band was significantly more intense in SOD1 with C⁴S mutations (Figure 6d), consistent with the favorable monomerization (Arnesano et al., 2004). Also, the cross-linked band was prominent in SOD1 with L144F mutation (Figure 6d), which is in line with the previous report showing the selective destabilization of the dimer interface in SOD1(L144F) (Lindberg et al., 2005). Again, no cross-linked bands at 30 kDa in the *E. coli* lysates were observed when using sh-hFN3 instead of Mb(S4) (Figure S5), confirming the applicability of Mb(S4) for the detection of monomeric SOD1 in the samples ex vivo.

Taken together, our crosslinking assay using Mb(S4) can probe the monomerization of SOD1 in cell lysates containing highly heterogeneous mixtures of proteins and suggest that the increased tendency of the

monomerization would be a feature of some but not all SOD1 variants with ALS-causing mutations.

3.6 | Structural consideration on the recognition of SOD1 by monobodies

In elucidating the structural basis for the interaction between SOD1 and monobodies, we examined the binding site on SOD1(MM) for the monobodies, referred to as an epitope region, by a yeast-surface display method and found that Mb(S2) and Mb(S4) competed with each other for the binding of SOD1(MM) (Figure S6). Therefore, the epitope region on SOD1 for Mb(S2) and Mb(S4) are considered to be overlapped.

To further characterize the epitope region on SOD1, we introduced into SOD1(MM) the additional

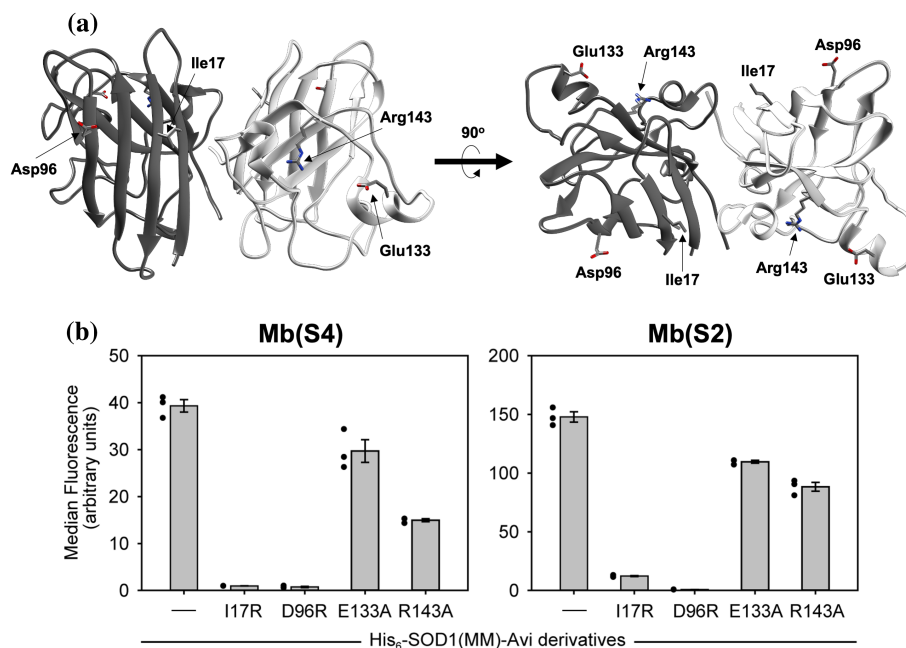


FIGURE 7 Examination of epitope region on SOD1 recognized by monobodies (a) The amino acid residues examined for the binding with monobodies (Ile17, Asp96, Glu133, and Arg143) are shown on each of the subunits of SOD1 (PDB ID: 1HL5). The structure shown left is the same orientation with that shown in Figure 1. (b) The binding of the indicated SOD1 variants with (left) Mb(S4) and (right) Mb(S2) was investigated by the yeast-surface display method. Biotinylated His₆-SOD1(MM)-Avi and its variants with indicated mutations in the concentration of 2 μ M were incubated with yeast cells displaying (left) Mb(S4) or (right) Mb(S2). The median fluorescence intensities are shown as the mean of three independent experiments with standard deviation.

substitution of arginine for the surface-exposed residues Ile17 and Asp96 on the β -sheet structure (I17R and D96R) (Figure 7a). Also, we noted two additional surface-exposed residues Glu133 and Arg143, which are positioned on the side of SOD1 opposite to Ile17 and Asp96 (Figure 7a), and replaced them with alanine in SOD1 (MM) (E133A and R143A). These substitutions did not significantly affect the secondary structures and also maintained the monomeric state of SOD1 (MM) (Figures S7 and S8). As shown in Figure 7b, the yeast-surface display assay revealed that I17R and D96R substitution in SOD1(MM) abrogated the interaction with both Mb(S2) and Mb(S4); in contrast, a SOD1 (MM) variant either with E133A or R143A was still able to interact with Mb(S2) and Mb(S4). While we also utilized ColabFold v.1.5.2 (Mirdita et al., 2022) in an attempt to predict the structure of the Mb(S2)/Mb(S4)-SOD1 complex, the resulting models in which Glu133/Arg143 but not Ile17/Asp96 forms the interaction interface could not describe our experimental results (Figure S9). Setting a threshold for weakened interaction at a 50% reduction in the median fluorescence intensity, Arg143 in SOD1 (MM) would be involved in the interaction with Mb(S4) but not with Mb(S2) (Figure 7b). Arg143 is located within a β -strand that forms part of the dimer interface in SOD1 (Figure 7a), which might hence

account for the specific binding of Mb(S4) to monomeric but not dimeric SOD1. Taken together, the primary epitope region on SOD1 for the interaction with our monobodies is presumed to be located on the side of the β -sheet structure, which is aligned with the preference of monobodies from the side library for a flatter surface characteristic of a β -sheet structure (Sha et al., 2017).

We also attempted to identify a region in Mb(S4) and Mb(S2) for the binding of SOD1, referred to as a paratope region. In the three-dimensional structure of Mb(S4) and Mb(S2), as predicted using ColabFold v1.5.2 and depicted in Figure 8a, most of the distinct residues between Mb(S4) and Mb(S2) marked in red are situated on the same face of the monobody. To examine the paratope regions of the monobodies for SOD1(MM), several residues constituting the face in the monobodies were selected for alanine substitution; namely, for Mb(S4), these include Asn44, Lys49, Tyr78, and Arg79; for Mb(S2), they are Tyr46, Glu48, Tyr79, and Arg80 (Figure 8a).

Using yeast cells expressing Mb(S4)/Mb(S2) with alanine substitutions on the surface, the yeast-surface display assay with biotinylated His₆-SOD1(MM)-Avi revealed that the binding of Mb(S4) with SOD1(MM) was little affected with the N44A mutation but almost completely abrogated with K49A, Y78A, and R79A

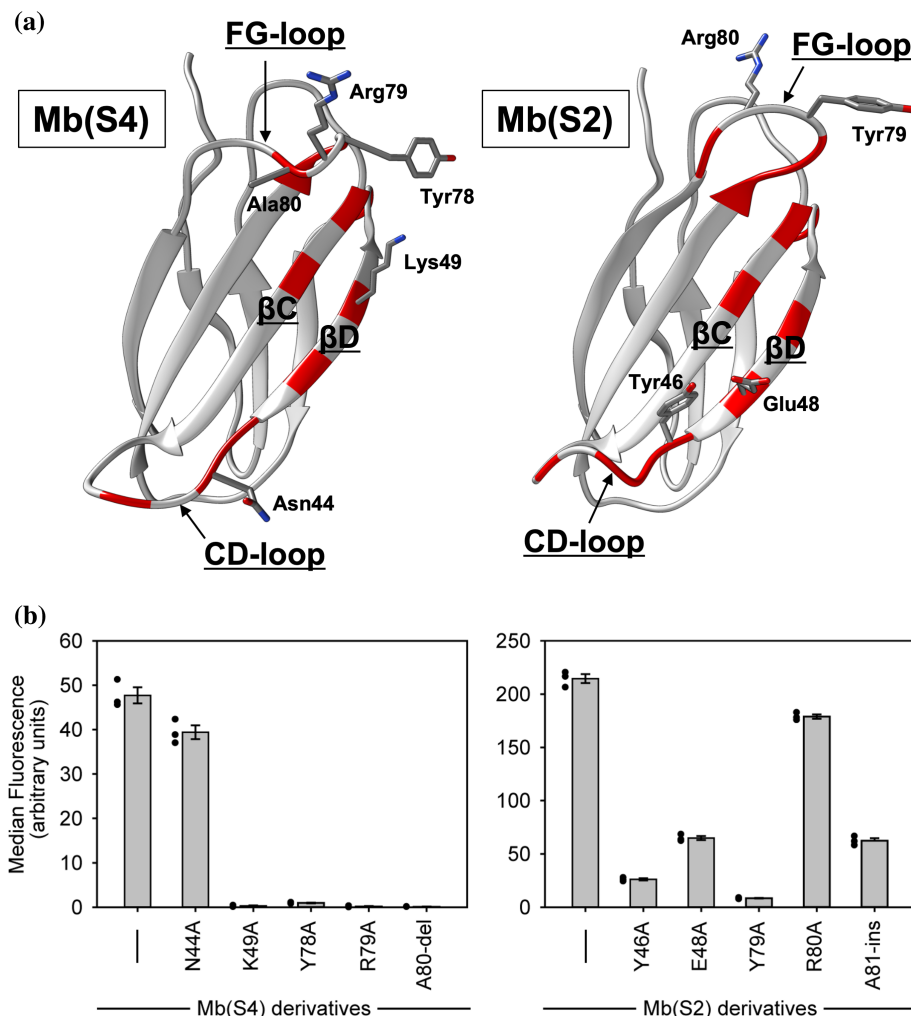


FIGURE 8 Examination of paratope regions on monobodies interacted with SOD1 (a) The structures of Mb(S4) and Mb(S2) predicted by ColabFold v1.5.2 are shown. The sites where the amino acid residues are different between Mb(S4) and Mb(S2) are colored red, and the amino acid residues examined for the binding of SOD1 are shown in a stick model. (b) The binding of SOD1(MM) with the indicated variants of (left) Mb(S4) and (right) Mb(S2) was investigated by the yeast-surface display method. Biotinylated His₆-SOD1(MM)-Avi in the concentration of 2 μ M were incubated with yeast cells displaying (left) Mb(S4) variants or (right) Mb(S2) variants with indicated mutations. The median fluorescence intensities are shown as the mean of three independent experiments with standard deviation.

mutation (Figure 8b). It is also notable that Mb(S1), a Mb(S4) variant with Y78F mutation, showed weaker affinity to SOD1(MM) than that of Mb(S4) (Figure 3b,c). In Mb(S2), in contrast, Y46A, E48A, and Y79A mutation were found to weaken the interaction with SOD1(MM), while the interaction was almost intact with R80A mutation (Figure 8b).

Based upon those results, we suggest that Mb(S4) binds monomeric SOD1 primarily through the region encompassed by the FG-loop and the β D strand, with almost no significant contribution from the CD-loop. In contrast, Mb(S2) seems to use the region encompassed by the CD-loop and the β D strand for the interaction with SOD1. The FG-loop in Mb(S2) was considered to play a critical role in the interaction but contribute to the binding of SOD1 in a manner distinct from that of Mb(S4). Considering that the FG-loop of Mb(S2) contains one less amino acid residue than that of Mb(S4) (Figure 3b), two additional variants were also tested for the interaction with SOD1(MM): a Mb(S4) variant with the deletion of Ala80 (A80-del) and a Mb(S2) variant with the insertion of an alanine residue

following Arg80 (A81-ins). As shown in Figure 8b, the interaction with SOD1(MM) was significantly weakened in the A81-ins variant of Mb(S2) and completely disrupted in the A80-del variant of Mb(S4). These results support the idea that the distinct amino acid sequences of FG-loops in Mb(S2) and Mb(S4) dictate specific conformations conducive to binding with SOD1(MM).

In spite of our effort to characterize the epitope and paratope regions, it remains to be considered how Mb(S4) but not Mb(S2) can discriminate between monomeric and dimeric forms of SOD1. While it is well expected that Mb(S4) can selectively recognize monomeric SOD1 by utilizing steric hindrance occurring with dimeric SOD1, structural analysis on the Mb(S4)–monomeric SOD1 complex is one of our on-going projects.

4 | CONCLUSIONS

In this study, we for the first time have developed a monobody specifically recognizing monomeric SOD1.

The monobody Mb(S4) was found to interact exclusively with the monomeric SOD1 but not the SOD1 homodimer, which was corroborated by the binding analysis with BLI as well as the yeast-surface display method. Contrary to the excellent specificity, the affinity of Mb(S4) with monomeric SOD1 was not so high (apparent $K_d \sim 5.0 \times 10^{-6}$ M) as compared with conventional antibodies having K_d values in nanomolar range. With the help of a proximity-enabled chemical crosslinking strategy, however, Mb(S4) successfully detected a fraction of the SOD1 monomer in some of the SOD1 variants with ALS-causing mutations in biological samples *ex vivo*. While the mechanistic details of the SOD1 monomer-specificity of Mb(S4) awaits further investigation on the Mb(S4)–SOD1 complex structure, the results here highlight the potential of monobodies for targeting the SOD1 monomer. With broad advantages of monobodies over conventional antibodies as stated above, we hope that the monobody-based detection system in conjunction with chemical crosslinking may find use in wide range of applications and thereby advance understanding of a pathomechanism of ALS.

AUTHOR CONTRIBUTIONS

Yoshiaki Furukawa: Conceptualization; funding acquisition; supervision; writing – original draft; writing – review and editing. **Hiroshi Amesaka:** Investigation; methodology; writing – review and editing. **Mizuho Hara:** Investigation. **Yuki Sakai:** Investigation. **Atsuko Shintani:** Investigation; validation. **Kaori Sue:** Investigation; validation. **Tomoyuki Yamanaka:** Investigation. **Shun-ichi Tanaka:** Conceptualization; funding acquisition; supervision; writing – original draft; writing – review and editing.

ACKNOWLEDGMENTS

We thank Dr. D. Fujita and Dr. Y. Nakura (Institute for Integrated Cell-Material Sciences at Kyoto University) for access to the flow cytometry used for yeast cell sorting and also acknowledge Mr. T. Seguchi (Sartorius Japan K.K) for discussion on the BLI results. This work was supported by Grants-in-Aid for Scientific Research on Innovative Areas (19H05765 to YF, and 20H05516 to ST), for Scientific Research (B) (22H02768 to YF), for Scientific Research (C) (21K05386 to ST), and for Challenging Exploratory Research (22K19389 to YF) from the Ministry of Education, Culture, Sports, Science and Technology of Japan.

ORCID

Shun-ichi Tanaka  <https://orcid.org/0000-0003-4270-0374>

Yoshiaki Furukawa  <https://orcid.org/0000-0002-1918-372X>

REFERENCES

- Arnesano F, Banci L, Bertini I, Martinelli M, Furukawa Y, O'Halloran TV. The unusually stable quaternary structure of human SOD1 is controlled by both metal occupancy and disulfide status. *J Biol Chem.* 2004;279:47998–8003.
- Bertini I, Piccioli M, Viezzoli MS, Chiu CY, Mullenbach GT. A spectroscopic characterization of a monomeric analog of copper, zinc superoxide dismutase. *Eur Biophys J.* 1994;23:167–76.
- Bruijn LI, Houseweart MK, Kato S, Anderson KL, Anderson SD, Ohama E, et al. Aggregation and motor neuron toxicity of an ALS-linked SOD1 mutant independent from wild-type SOD1. *Science.* 1998;281:1851–4.
- Forman HJ, Fridovich I. On the stability of bovine superoxide dismutase. The effects of metals. *J Biol Chem.* 1973;248:2645–9.
- Fujita J, Amesaka H, Yoshizawa T, Hibino K, Kamimura N, Kuroda N, et al. Structures of a FtsZ single protofilament and a double-helical tube in complex with a monobody. *Nat Commun.* 2023;14:4073.
- Furukawa Y. Good and bad of Cu/Zn-superoxide dismutase controlled by metal ions and disulfide bonds. *Chem Lett.* 2021;50:331–41.
- Furukawa Y, O'Halloran TV. Amyotrophic lateral sclerosis mutations have the greatest destabilizing effect on the apo, reduced form of SOD1, leading to unfolding and oxidative aggregation. *J Biol Chem.* 2005;280:17266–74.
- Furukawa Y, Torres AS, O'Halloran TV. Oxygen-induced maturation of SOD1: a key role for disulfide formation by the copper chaperone CCS. *EMBO J.* 2004;23:2872–81.
- Hantschel O, Biancalana M, Koide S. Monobodies as enabling tools for structural and mechanistic biology. *Curr Opin Struct Biol.* 2020;60:167–74.
- Hayashi Y, Homma K, Ichijo H. SOD1 in neurotoxicity and its controversial roles in SOD1 mutation-negative ALS. *Adv Biol Regul.* 2016;60:95–104.
- Helma J, Cardoso MC, Muyldermans S, Leonhardt H. Nanobodies and recombinant binders in cell biology. *J Cell Biol.* 2015;209:633–44.
- Khare SD, Caplow M, Dokholyan NV. The rate and equilibrium constants for a multistep reaction sequence for the aggregation of superoxide dismutase in amyotrophic lateral sclerosis. *Proc Natl Acad Sci U S A.* 2004;101:15094–9.
- Koide A, Bailey CW, Huang X, Koide S. The fibronectin type III domain as a scaffold for novel binding proteins. *J Mol Biol.* 1998;284:1141–51.
- Koide A, Wojcik J, Gilbreth RN, Hoey RJ, Koide S. Teaching an old scaffold new tricks: monobodies constructed using alternative surfaces of the FN3 scaffold. *J Mol Biol.* 2012;415:393–405.
- Lindberg MJ, Bystrom R, Boknas N, Andersen PM, Oliveberg M. Systematically perturbed folding patterns of amyotrophic lateral sclerosis (ALS)-associated SOD1 mutants. *Proc Natl Acad Sci U S A.* 2005;102:9754–9.
- Mirdita M, Schutze K, Moriwaki Y, Heo L, Ovchinnikov S, Steinegger M. ColabFold: making protein folding accessible to all. *Nat Methods.* 2022;19:679–82.
- Mulligan VK, Kerman A, Ho S, Chakrabarty A. Denaturational stress induces formation of zinc-deficient monomers of Cu,Zn superoxide dismutase: implications for pathogenesis in amyotrophic lateral sclerosis. *J Mol Biol.* 2008;383:424–36.

- Nakamura I, Amesaka H, Hara M, Yonezawa K, Okamoto K, Kamikubo H, et al. Conformation state-specific monobodies regulate the functions of flexible proteins through conformation trapping. *Protein Sci.* 2023;32:e4813.
- Rakhit R, Robertson J, Vande Velde C, Horne P, Ruth DM, Griffin J, et al. An immunological epitope selective for pathological monomer-misfolded SOD1 in ALS. *Nat Med.* 2007;13:754–9.
- Redler RL, Wilcox KC, Proctor EA, Fee L, Caplow M, Dokholyan NV. Glutathionylation at Cys-111 induces dissociation of wild type and FALS mutant SOD1 dimers. *Biochemistry.* 2011;50:7057–66.
- Rosen DR, Siddique T, Patterson D, Figlewicz DA, Sapp P, Hentati A, et al. Mutations in Cu/Zn superoxide dismutase gene are associated with familial amyotrophic lateral sclerosis. *Nature.* 1993;362:59–62.
- Sha F, Salzman G, Gupta A, Koide S. Monobodies and other synthetic binding proteins for expanding protein science. *Protein Sci.* 2017;26:910–24.
- Tajiri M, Aoki H, Shintani A, Sue K, Akashi S, Furukawa Y. Metal distribution in Cu/Zn-superoxide dismutase revealed by native mass spectrometry. *Free Radic Biol Med.* 2022;183:60–8.
- Tanaka S, Takahashi T, Koide A, Ishihara S, Koikeda S, Koide S. Monobody-mediated alteration of enzyme specificity. *Nat Chem Biol.* 2015;11:762–4.
- Tanaka SI, Takahashi T, Koide A, Iwamoto R, Koikeda S, Koide S. Monobody-mediated alteration of lipase substrate specificity. *ACS Chem Biol.* 2018;13:1487–92.

SUPPORTING INFORMATION

Additional supporting information can be found online in the Supporting Information section at the end of this article.

How to cite this article: Amesaka H, Hara M, Sakai Y, Shintani A, Sue K, Yamanaka T, et al. Engineering a monobody specific to monomeric Cu/Zn-superoxide dismutase associated with amyotrophic lateral sclerosis. *Protein Science.* 2024;33(4):e4961. <https://doi.org/10.1002/pro.4961>